ENGINEERING TRANSACTIONS • *Engng. Trans.* • **42**, 1–2, 61–74, 1994
Polish Academy of Sciences • Institute of Fundamental Technological Research

STABILITY OF THE CYLINDRICAL PANEL. EXPERIMENTAL INVESTIGATIONS AND NUMERICAL ANALYSIS

J. MARCINOWSKI and D. ANTONIAK (WROCŁAW)

The steel shallow cylindrical shell subjected to the action of a concentrated force applied at its center is the subject of the experimental test and numerical analysis. Both investigations were performed within the large deformation range. At the same time strains and stresses remained small enough to ensure purely elastic material changes within the shell. Special attention was focussed on the stability phenomena. The fundamental equilibrium paths with all critical points as well as the postbuckling path were determined numerically. This solution was compared with the equilibrium path obtained in the experiment. Satisfactory agreement of the obtained solutions confirmed the correctness and versatility of the program used in the numerical analysis. The conclusions drawn from the comparative analysis performed are presented in the paper.

1. INTRODUCTION

Very fast and large (in the sense of processor speed, memory and hard disk capacity) computers which are at present in common use enable us to perform the numerical analysis of arbitrary structures within the arbitrary range of strains and displacement. Of course, besides the computer, also the program which is capable of performing such an analysis is needed as well. Here the problem of reliability of the obtained results appears. How can they be verified? It is possible to compare the solution obtained with the results given by other authors who used other computer programs. But it would be only a comparison of two different codes for the same calculation model. The best verification of both the mathematical and the physical models and the code correctness would be the comparison with the real object behaviour. This very comparison analysis was performed and its results are presented in the paper.

The cylindrical panel loaded by a concentrated force at the center exhibits many interesting features from the point of view of stability analysis. This is the reason why it is so frequently analyzed by many authors, cf. [1, 2, 3, 4, 5]. In these works the shell of a considerable thickness is considered. Shells of that type are very regular as far as the deformation is concerned.

Their numerical analysis is comparatively simple. Here a very thin shell is analyzed. All equilibrium paths are very complicated and so is the whole numerical and experimental analysis. The fundamental equilibrium paths exhibit many extremes, loops and turning points. The looping phenomenon was observed and confirmed the earlier results obtained by TSAI and PALAZOTTO [6] for the panel of the radius-to-thickness ratio smaller than for the panel considered here.

The preparation of the testing apparatus and the specimen itself is very expensive and time-consuming. Preparation of the cylindrical panel is comparatively simple and inexpensive. This is the reason why we have selected this very shell as the subject of comparative analysis.

Besides this principal aim (the comparative analysis), the project had also certain cognitive reasons. Investigation of stability of a spatial structure with imperfections is a very interesting task, not only for somebody who deals with the stability problems.

2. EXPERIMENTAL TESTS

2.1. Description of the testing apparatus

The experiment concerned large deformations of the shell, the dimensions, loading and support conditions of which are shown in Fig. 1. The

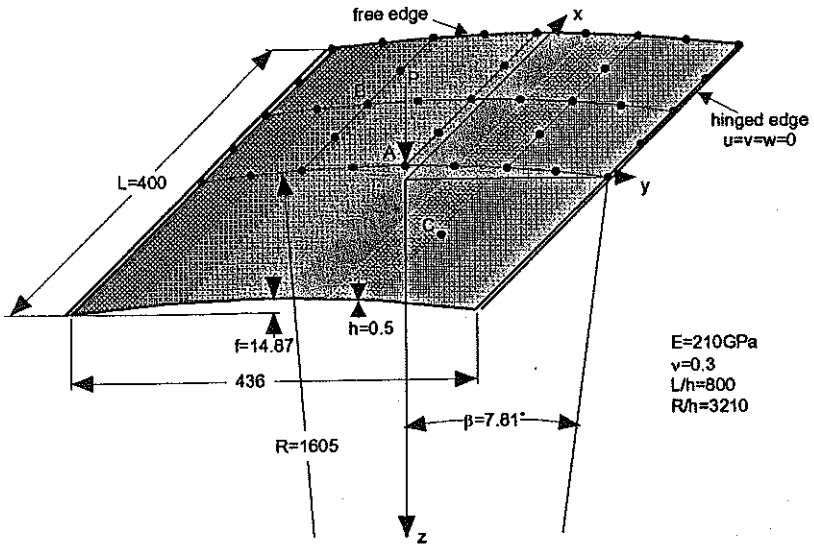

FIG. 1. Scheme of the examined panel.

scheme of the testing apparatus is presented in Fig. 2. The shell is made of high-strength steel and its form was obtained by cold rolling. The rectilinear edges of the shell are supported in vee grooves (*4*, Fig. 2) enabling free rotation of the shell. The grooves are cut in solid channel bars *(2)* joined to a rigid laboratory table. Sensor of a force gauge *(5)* and sensors of two inductive displacement gauges *(6* and *7)* are attached to a rigid external frame. The third dial displacement gauge *(8)* is placed under the shell. Displacements of the center of the shell are measured by this gauge. Displacements of the central point of the shell are introduced by a screw-jack *(9)* located between the force gauge and the central point of the shell. The additional dial displacement gauge *(10)* was suitably placed to control the horizontal motion of the supporting channel bars and to verify that the supports were really rigid.

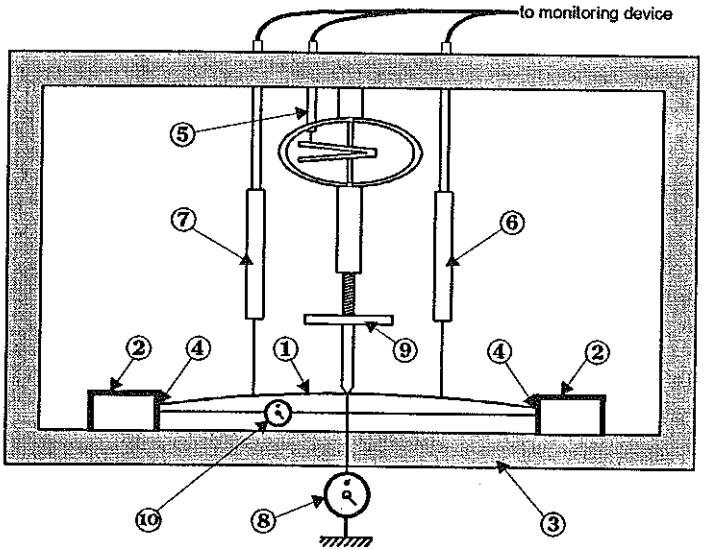

FIG. 2. Testing apparatus scheme.

2.2. Description of the experiment

The principal aim of the experiment was the measurement of nonlinear equilibrium paths of three shell points A, B and C (Fig. 1).

Changing the displacement of the central point by the screw-jack *(9)* allowed to introduce various deformations in the shell. After each increment of the displacement, readings of the force and displacement gauges were taken. The force gauge data enabled us to evaluate the load corresponding to the actual state of displacement. As increasing displacements were introduced,

successive points on the equilibrium paths were obtained. At a certain instant of the process the sign of the load changed; however, the continuation of the experiment was still possible since the screw-jack was attached to the shell with a nut. Observations were conducted until the shell snapped through and became inverted. The experimentally recorded paths (line with markers) are plotted together with the numerically determined paths (lines without markers) in Figs. 3 and 6. The experiment was repeated several times. The dominating form of the stability loss was bifurcation followed by bulging of the left-hand side of the shell.

3. Calculation of nonlinear equilibrium paths

In the numerical investigations the program described in details in [3] was utilized. The finite element method was used to discretize the shell domain. The curved isoparametric finite element introduced by Ahmad *et al.* [7] and supplemented in [8], [9] after appropriate developing [3] was applied to the nonlinear analysis in the program used. Due to the symmetry of the deformation observed in the experimental test, only one half of the shell was divided into finite elements. This division is shown in Fig. 1. There are five degrees of freedom (three displacements in global coordinates and two independent rotations) in every node. This division leads to 185 degrees of freedom.

The numerical analysis started from tracing the fundamental path. This path corresponds to the symmetric form of deformation. The fundamental path was determined only in the initial stage since then its characteristics proved to be very complicated.

During the analysis only displacements were used as control parameters; they were changed in the cases when the convergence became worse. In the program the displacement control parameter and its increment were chosen automatically (the first two steps are an exception from this rule) on the basis of the two former steps. The best choice of the control parameter fulfils the condition

$$\frac{\Delta d^m_{i-1}}{\Delta d^m_{i-2}} \quad \text{is a maximum,}$$

where Δd^m_{i-1} is the increment of the d^m parameter in the $(i-1)$ step. The increment of the control parameter is the fraction of Δd^m_{i-1} and depends on the number of iterations in the $(i-1)$ step.

It should be mentioned that translations as well as rotations were used to control the tracing process. All the time the sign of the determinant of

the stiffness matrix was monitored. At the very beginning it was positive; its change was the signal that the type of equilibrium state had changed.

The first change of the stability determinant encountered on the increasing portion of the path proved that the bifurcation point was passed. The determination of its accurate location was postponed for further analysis (see below).

The most important portions of the fundamental path for node A are presented in Fig. 3 by a solid line. It presents the set of all equilibrium configurations, independently of their being stable or not. The initial portion (below point B_1) and the final one (above point B_2) are stable. The remaining configurations are unstable. The final portion corresponds to the inverted form of the panel; it is stable and comparatively very stiff (the path is nearly vertical). The view of the inverted configurations and its contour maps are shown in Figs. 4 and 5. This configuration was labelled by the number *1* in Fig. 6. The most important parts of the fundamental path for the node B (Fig. 1) of the panel are shown in Fig. 6 by a solid line.

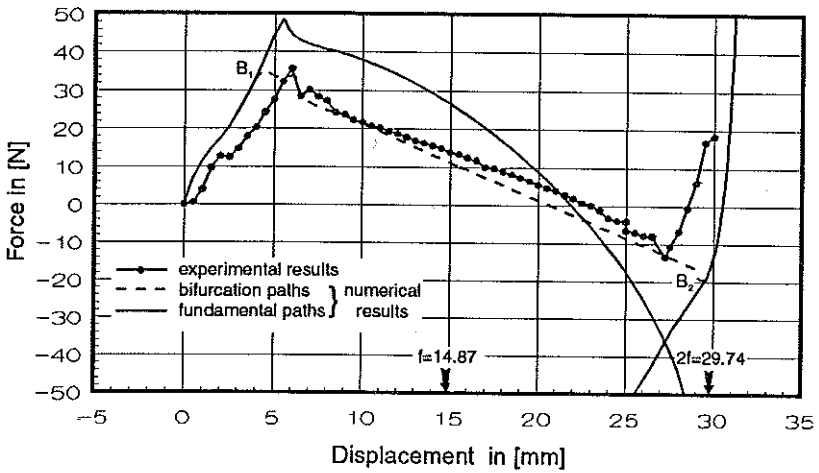

FIG. 3. Equilibrium paths on the $u_Z^A - \lambda$ plane.

At the next step of the numerical analysis the location of the bifurcation points and both bifurcation paths were determined. The procedure called the load perturbation approach [10] was adopted here. This numerical procedure proceeded as follows. First the perturbation force equal to 0.05 was applied at the node, to the right of point A and directed downwards. The imperfection path corresponding to this perturbation force (with the main loading, of course) was traced to the level of the first bifurcation point (point B_1). Strictly speaking, it was traced to the level a little bit above that level. Then the perturbation load was removed. After a few additional iterations

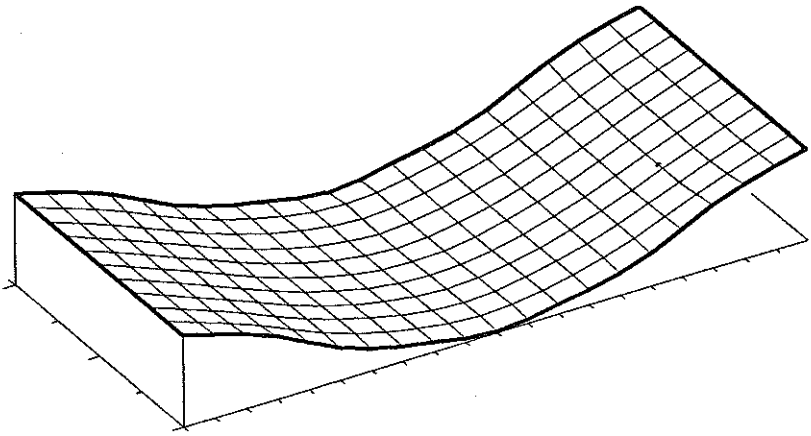

FIG. 4. View of the deformed panel.

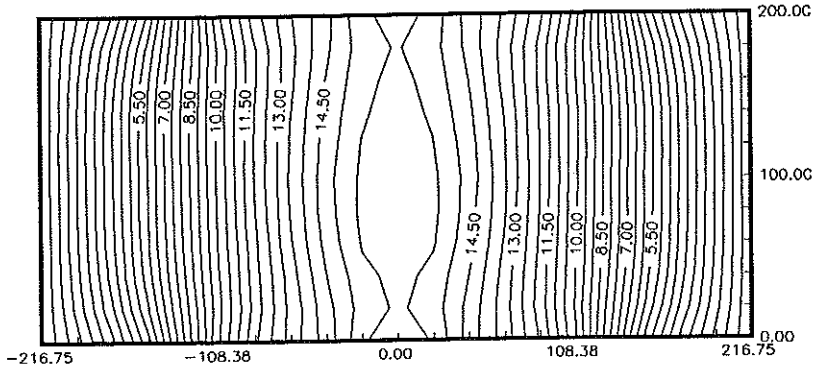

FIG. 5. Contour map of the deformed panel.

the first configuration on the postbuckling path was found. The further tracing process of the postbuckling path proceeded in the same way as the calculation of the fundamental path.

The accurate location of the bifurcation point was determined as the point of intersection of the fundamental and postbuckling paths. In the same manner the second bifurcation point (B_2) was determined.

The dashed line in Fig. 3 represents the postbuckling paths of the node A. These are really two paths, in spite of the fact that in this figure only one path is seen. It is the projection on the subspace and in this projection both paths coincide. In Fig. 6 both postbuckling paths of node B are shown by dashed lines. They form a characteristic loop.

The configuration labelled *2* in Fig. 6 is shown in Fig. 7 and is presented as the contour map in Fig. 8. The antisymmetric form of deformation is visible. On the second postbuckling path the form of deformation will be exactly opposite.

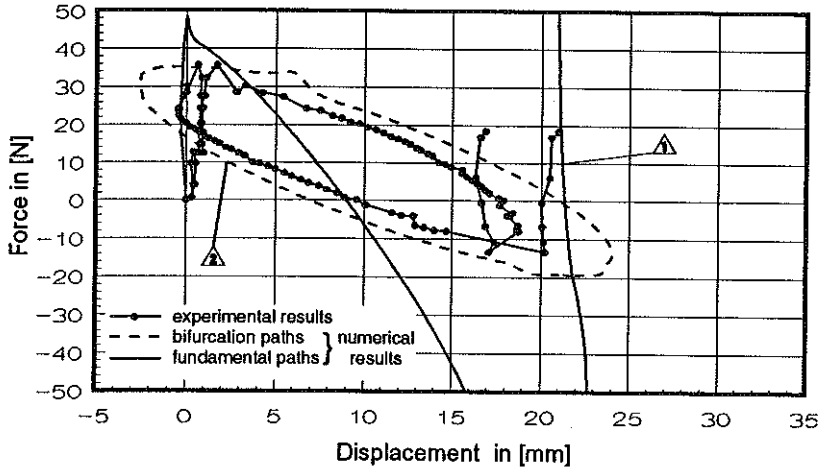

FIG. 6. Equilibrium paths on the $u_Z^B - \lambda$ plane.

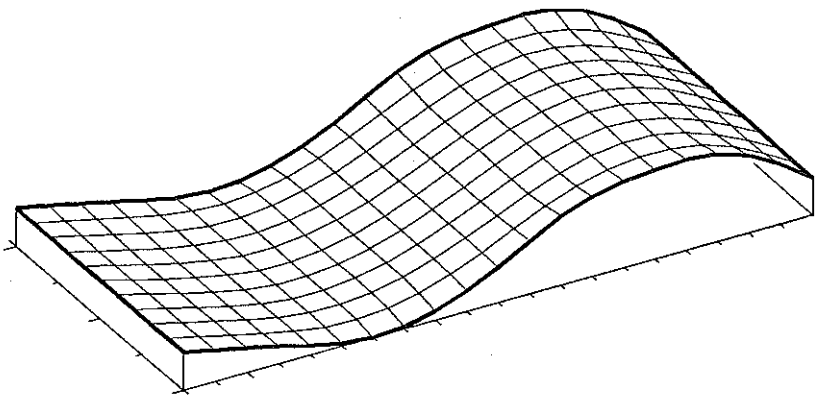

FIG. 7. View of the antisymmetrically deformed panel.

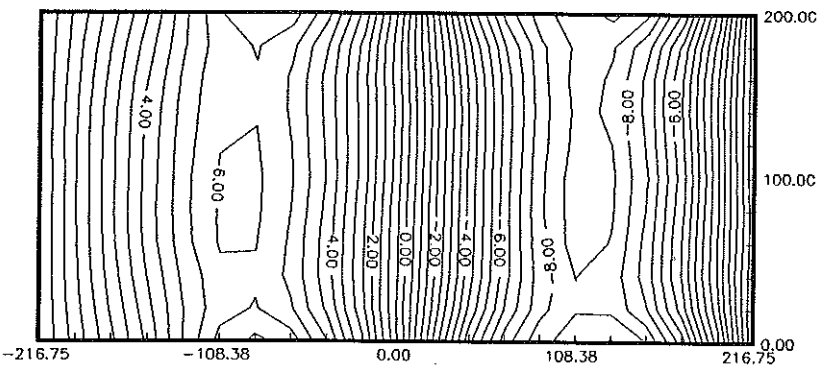

FIG. 8. Contour map of the antisymmetrically deformed panel.

The solution obtained enables us to describe the phenomenon of stability loss which may take place. Immediately after the concentrated force exceeds the value corresponding to the first bifurcation point (B_1), the panel will buckle into an unsymmetric form. This configuration being unstable, further sudden movement of the panel will terminate at any point on the final portion of the fundamental path. It means that the final configuration will be the inverted configuration.

The final portion of the fundamental path was determined by a smooth transition from the postbifurcation path. The antisymmetric form of deformation (which characterized the deformation on the postbifurcation path) changes at a certain point into a symmetric form. The sign of the tangent stiffness matrix becomes positive and this is a signal that the return to a stable configuration on the fundamental path occurs.

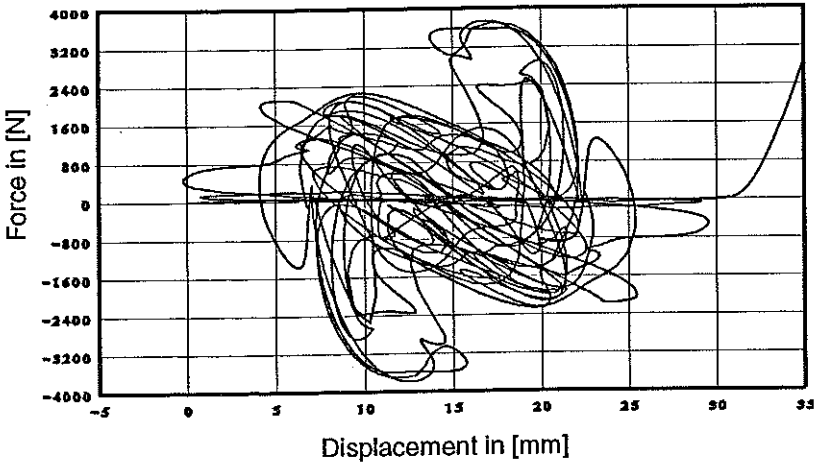

FIG. 9. Fundamental equilibrium path on the $u_Z^A - \lambda$ plane.

The complete fundamental path was determined independently, on the basis of division of one quarter of the shell into four elements, what leads to a discrete system of 105 degrees of freedom. The entire fundamental path was calculated within the whole range of load variation. Figures 9 and 10 present the fundamental paths of nodes A and B. In the initial and final portions they coincide with the charts previously obtained (Figs. 3 and 6). A comment is necessary regarding extremely numerous unstable configurations lying between those two stable limit ranges. In the Figs. 11 and 12 the same charts are presented in a different form, i.e. according to the arc parameter. This allowed us to obtain slightly more convenient images of those curves presenting their essential features. It is easy to find the center of symmetry about which the corresponding branches of equilibrium paths propagate.

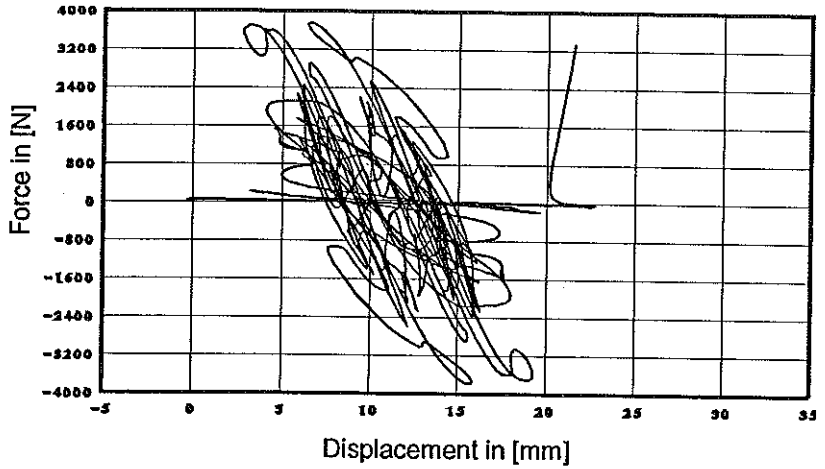

FIG. 10. Fundamental equilibrium paths on the $u_Z^B - \lambda$ plane.

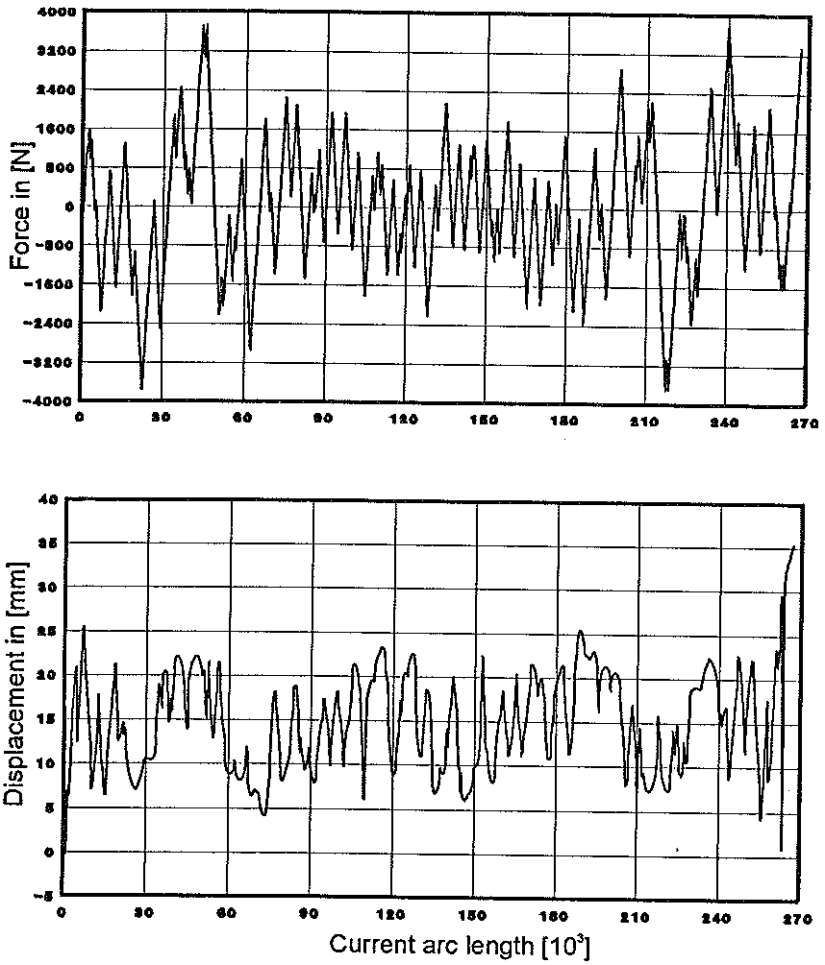

FIG. 11. Fundamental path on the $u_Z^A - \lambda$ plane versus current arc parameter.

This indicates that, in spite of the initial curvature, the response of the shell in both directions (up and down) is almost identical.

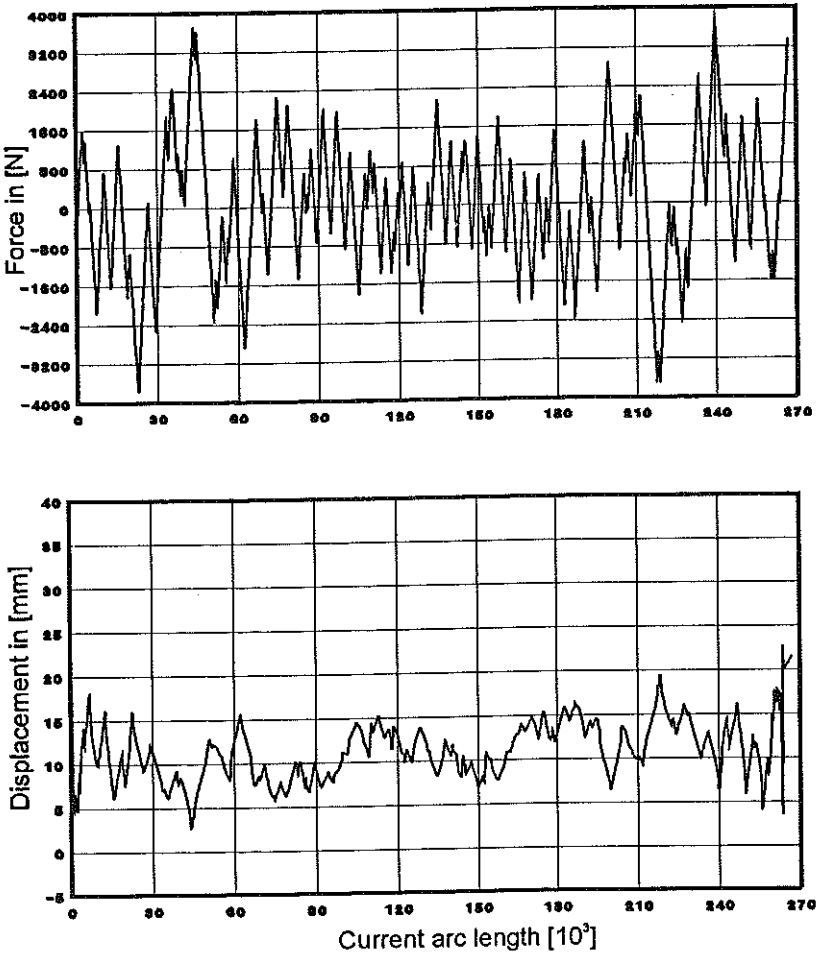

FIG. 12. Fundamental path on the $u_Z^B - \lambda$ plane versus current arc parameter.

Large number of unstable configurations and the loops of the fundamental path in the unstable range may be difficult to understand. Unfortunately, it is not easy to explain them on the basis of other publications. In this context let us mention the comparative analysis of a shell with similar geometry published by RADWAŃSKA [4]. In that paper the equilibrium paths of a shell with comparable geometry and equivalent load were determined numerically. The equilibrium paths of the central point of the shell for five different thicknesses are presented on page 173. A tendency of increasingly complicated paths for thinner shells is easily observed. The thinnest shell

L/h and R/h–ratios were equal to 79.4 and 400, while the rise f was equal to 12.7 mm. A similar conclusion can be drawn from the results presented in [6]. The geometric parameters of the shell considered there were the following: $L/h = 40$, $R/h = 200$ and $f = 50.8$ mm. The corresponding parameters of the shell examined in this paper were, respectively, 800 and 3210 for $f = 14.87$ mm, what exceeds the values considered in [4] and [6].

To examine the dependence of the path on the mesh density, the path was also determined (in a limited range) for a division of 9 (200 dof) and 16 (325 dof) finite elements (a quarter of the shell). The tendency of the fundamental path with a center of symmetry to form the loops was also observed in [4]. The result of the comparison made for various mesh densities is presented in Fig. 13. Up to the point C, all three curves coincide. At this point the curve *1* splits, but curves *2* and *3* still coincide until point D is reached. Then also these curves are distinct. Further differences are observed mainly in the values of the extrema reached and the smoothness of curves.

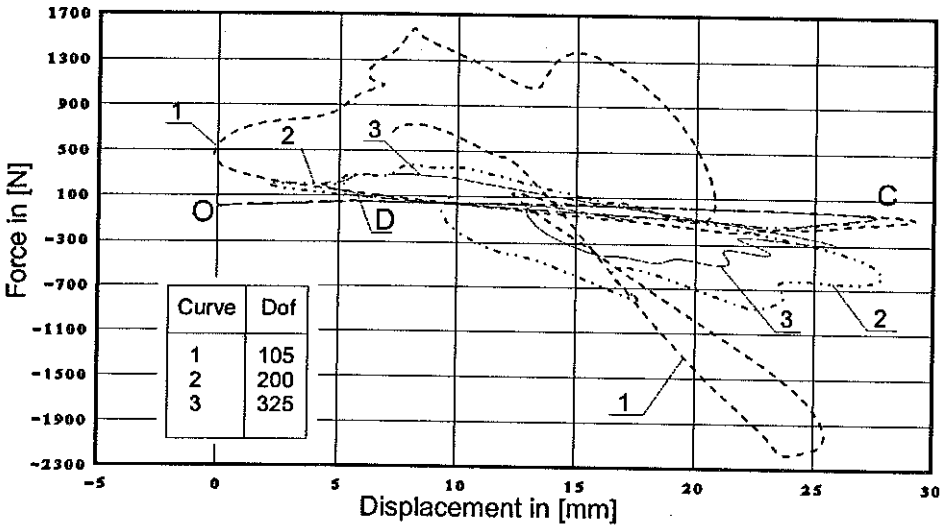

FIG. 13. Fundamental equilibrium paths on the $u_z^A - \lambda$ plane.

This additional numerical calculations allowed us to confirm the fact that there really exist numerous unstable configurations which create characteristic loops in the load-displacement space. This conclusion could be drawn even on the basis of these simple calculations. One can expect that, even for more refined meshes, the observed differences will concern the extremal values and the curve smoothness (compare curves *2* and *3* in Fig. 13).

One must say that, as far as this range is concerned, the mesh corre-

sponding to 105 dof is not appropriate. The mesh corresponding to 325 dof may be quite satisfactory. There was no need to trace the fundamental path in its whole range using such a fine division. From the engineering point of view this range is not so important as the initial and final parts of the load-displacement history. Since within the initial range ($0 - C$ interval in Fig. 13) all three curves coincide, it means that the solutions presented in Fig. 3 to 8 are quite satisfactory as far as the mesh is concerned. Frankly speaking, there was no possibility to obtain such solutions for finer meshes due to hardware capabilities (all computations were performed on a PC 386 and 486).

4. Final remarks and conclusions

Generally speaking, one can say that the comparative analysis performed yielded satisfactory results. Plots obtained as the result of the numerical analysis should be referred to the ideal structure without geometric imperfections. This ideal geometry was established by averaging the shape of the several sections. The panel was not perfectly symmetric (a slight bulge of the left-hand side), and this was the reason why a such form of buckling dominated in several tests. It is obvious that the equilibrium paths obtained experimentally are the imperfection paths. Instead of the bifurcation points, the limit points appear and this is a rule. Bifurcation points are the attributes of ideal structures. In a real structure, i.e. a structure with imperfections, only limit points occur [11,12].

It should be emphasized that all configurations on the postbuckling paths are unstable. To answer the question, what kind of bifurcation point were those encountered on the fundamental path, two additional diagrams were done. In Figs. 14 and 15 bifurcation and fundamental equilibrium paths for the node A are shown. The first one refers to the horizontal translation of the node, the second one – to the rotation ϕ_x of this node. Both parameters remain active only along the bifurcation paths. Along the bifurcation paths all equilibrium configurations are unstable. The very narrow zones near the local maximum is the exception from this rule. From this fact and from Figs. 14 and 15 it follows that both bifurcation points encountered on the fundamental paths are unstable symmetrical points of bifurcation [11,12].

Of course, it was not possible to verify experimentally the unstable configurations obtained numerically in the form of numerous loops. The examined panel behaves regularly according to the existing imperfections. Only such a response to the load applied could be observed.

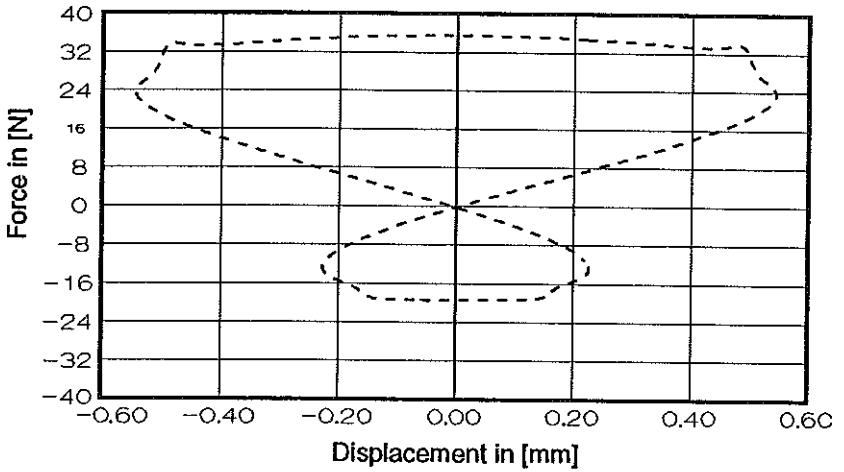

FIG. 14. Equilibrium paths on the $u_V^A - \lambda$ plane.

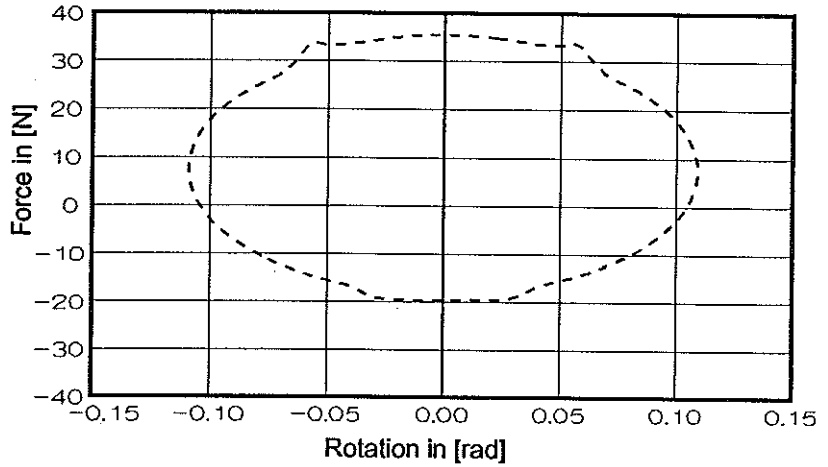

FIG. 15. Equilibrium paths on the $\phi_X^A - \lambda$ plane.

Even though several tests were performed on the same panel, no significant permanent deformations were registered. It means that really all deformations were purely elastic and the linearly elastic material model adopted in the program was adequate to our needs.

Imperfections are the main reason for the insignificant inconsistency between the numerical and the experimental investigations. To check if the mesh size was sufficient, the additional calculation of the fundamental path for division corresponding to 200 and 325 degrees of freedom (for a quarter of the shell) in its most important portion was made; the results prove that the adopted mesh was quite sufficient.

The numerical analysis was performed on typical PC (of the 386 and 486 family), though one must say that a faster computer (mainframe on a work-station) would be more adequate to the analysis of the problem discussed in the paper.

REFERENCES

1. M. A. CRISFIELD, *A fast incremental iterative solution procedure that handles "snap-through"*, Comp. Struct., **13**, 55–62, 1981.
2. T. MATSUI, O. MATSUOKA, *A new finite element scheme for instability analysis of thin shells*, Int. J. Num. Meth. Engng., **10**, 145–170, 1976.
3. J. MARCINOWSKI, *Calculation of the nonlinear equilibrium paths of the structures* [in Polish], Arch. Inż. Ląd. **35**, 3–4, 283–297, 1989.
4. M. RADWAŃSKA, *Large deformations and stability analysis of space structures by FEM* [in Polish], Wyd. Politechniki Krakowskiej, 1990.
5. W.B. KRÄTZIG, Y. BASAR, U. WITTEK, *Nonlinear behaviour and elastic stability of shells. Theoritical concepts. Numerical computations. Results*, [in:] Buckling of Shells, [Ed.] E. RAMM, Proc. State Art Colloq., Universität Stuttgart, Germany, May 6-7 1982, Springer-Verlag, 1982.
6. C.T. TSAI, A.N. PALAZOTTO, *Nonlinear and multiple snapping responses of cylindrical panels comparing displacements control and Riks method*, Comp. and Struc., **41**, 4, 605–610, 1991.
7. S. AHMAD, B.M. IRONS, O.C. ZIENKIEWICZ, *Analysis of thick and thin shell structures by curved finite elements*, Int. J. Num. Meth. Engng., **2**, 419–451, 1970.
8. S.F. PAWSEY, R.W. CLOUGH, *Improved numerical integration of thick shell finite elements*, Int. J. Num. Meth. Engng., **3**, 575–586, 1971.
9. O.C. ZIENKIEWICZ, R.L. TAYLOR, J.M. TOO, *Reduced integration technique in general analysis of plates and shells*, Int. J. Num. Meth. Engng., **3**, 275–290, 1971.
10. J.L. BATOZ, G. DHATT, *Incremental displacement algorithms for nonlinear problems*, Int. J. Num. Meth. Engng., **14**, 1262–1267, 1979.
11. K. HUSEYIN, *Nonlinear theory of elastic stability*, Noordhoff Inter. Publ., Leyden 1975.
12. J.M.T. THOMSON, G.W. HUNT, *A general theory of elastic stability*, J. Wiley and Sons, 1973.

WROCŁAW UNIVERSITY OF TECHNOLOGY
INSTITUTE OF CIVIL ENGINEERING, WROCŁAW.

Received August 19, 1993.